

SLAC-PUB-5217
March 1990
(A)

HIGH-RESOLUTION SIMULATION OF FIELD EMISSION*

W. B. HERRMANNSFELDT
*Stanford Linear Accelerator Center
Stanford University, Stanford, California 94309, USA*

REINARD BECKER
University of Frankfurt, D-6000 Frankfurt am Main, W. Germany

IVOR BRODIE, ARNE ROSENGREEN, and C. A. SPINDT
SRI International, Menlo Park, California 94025, USA

*Contributed to the Third International Conference on Charged Particle Beams,
Toulouse, France, April 24-27, 1990*

*Work supported by US Department of Energy contract DE-AC03-76SF00515 (SLAC).

Abstract

High-resolution simulations of field emission electron sources have been made using the electron optics program EGN2. Electron emission distributions are made using the Fowler–Nordheim equation. Mesh resolution in the range of 1–5 Å is required to adequately model surface details that can result in emission currents in the range found experimentally. A typical problem starts with mechanical details with dimensions of about 1 μm. To achieve high resolution a new boundary is defined by the tip, a nearby equipotential line, and a pair of field lines. The field lines (one of which is normally the axis of symmetry) define Neumann boundaries. This new boundary is then used by the boundary preprocessor POLYGON to create an enlarged version of the problem, typically by a factor of ten. This process can be repeated until adequate resolution is obtained to simulate surface details, such as a microprotusion, that could sufficiently enhance the surface electric fields and cause field emission.

When simulating experimental conditions under which emission of several microamperes per tip were observed, it was found that both a locally reduced work function and a surface protrusion were needed to duplicate the experimental results. If only a local region of reduced work function is used, the area involved and the extent of the reduction both need to be very large to reproduce the observed emission. If only a surface protrusion is used, it is possible to get the observed emission current with a reasonable protrusion of length a few times radius, but then the resulting beam spreads over a very large solid angle due to the strong local radial electric fields.

I. Introduction

This paper has two objectives:

- (1) To illustrate the techniques of magnifying the details of a region being simulated for Poisson's Equation, and subsequent raytracing to the extent necessary to directly apply the Fowler-Nordheim equation [1] to determine emission density and distribution.
- (2) To test the predictions of different assumed surface shapes and work function distributions to find results that agree with observations.

The experimental conditions that were simulated are similar to the gated field emitters used by Spindt [2] et al. Typically they find emission of a few microamperes per tip with about 100 V on the gate. The observed current distribution is uneven, leading to the conclusion that a number of small regions are emitting anomalously rather than in a generally uniform emission from the entire tip surface.

The simulations were made with the SLAC Electron Trajectory Program EGN2 [3] as converted to the language C and run on an IBM-type PC. The boundary input preprocessor program POLYGON [4] was used to define the boundaries and to perform the necessary magnifications. POLYGON contains a "zoom" feature that can expand and translate a region of a problem into a boundary dataset that contains the new boundary input data. Inputs to POLYGON are comprised of a combination of manually punched points, and data generated by EGN2 from the previous problem.

2. Techniques of Enhancing Resolution

This section is intended to demonstrate the methods by which successively higher resolution can be used to find the field distribution on the surface of a small point. A feeling for the magnitudes involved can be obtained by considering that the typical

dimensions of the gated field emitters are about $1\ \mu\text{m}$ in both the height of the emitter and the radius of the hole. The resolution needed to find the surface fields to the necessary accuracy is about $10^{-10}\ \text{m}$; thus to simulate only the first few micrometers of the beam, one would require much more than 10^8 mesh units.

The requirement for such high resolution stems from the need to be able to smoothly interpolate from the nearest mesh point to the surface along the smallest details deemed significant. The field-solving and partial routines are typically accurate to second-order in the spatial coordinates. Because potentials change so rapidly in the immediate proximity to a sharp point, it is necessary to have a mesh small compared to the dimensions of the point.

The gated field emitters typically resemble those shown in the microphotograph of fig. 1. In fig. 2 a single point and a small segment of the gate are shown with an extension to the right to simulate the presence of a drift region. In typical tests this drift region is about 1 mm long and is terminated by a surface about 1 kV above the gate potential. The right side of fig. 2 is terminated by an equipotential surface to maintain a uniform field of 1 kV/mm in the drift space. As noted on the figure, the resolution used is $0.05\ \mu\text{m}$ and the gate voltage is 100 V. The upper boundary is a Neumann boundary in both the zone between the base and the gate, and in the drift region. The limited Neumann condition used in EGN2 is that the normal field component is zero.

Figure 2 shows several equipotential lines and a single field line from the cone to near the inner edge of the gate electrode. The plan is to form a new boundary using the field line as a general Neumann boundary and an equipotential line as a "virtual anode." The method by which output from EGN2 is specified for POLYGON is described in sec. 3. In fig. 3 the boundary found from fig. 2 has been expanded by a factor of ten by using the zoom feature of POLYGON. Again a single field line has been generated with the

intention of creating another expanded boundary. Figure 4 shows the next enlargement, again by a factor of ten from the previous stage. The boundary near the tip of fig. 4 shows a small bump, which will be enlarged in detail in the next magnification. Again using the single field line from fig. 4 and the second of the two equipotential lines that are very close together, a new boundary dataset is generated, this time with an enlargement factor of five. Figure 5 shows the final stage of enlargement including a small bump with a radius of five mesh units, where the mesh is now 1 \AA .

The trajectories shown in fig. 5 were generated using the GENCARD feature of EGN2. In this mode the user specifies the starting coordinates of a particle, and EGN2 calculates the rest of the initial conditions including the current assigned to that particle. By specifying the work function and the field enhancement factor β , the user signals EGN2 to employ the dc formulation of the Fowler–Nordheim equation. An arbitrary decision has to be made by the user to determine the maximum angle, measured from the axis along the surface of the bump, for which emission will be calculated. Emission drops very quickly as a function of surface field with the Fowler–Nordheim equation, but the current is also proportional to the annular area assigned to each particle, so that trajectories emitted at fairly large angles contribute significantly. The trajectories in fig. 5 were limited to those with 50% or more of the peak current per ray. Note that the positions were chosen with equal spacing between rays.

The problem of determining the actual beam trajectories for the entire system now simply requires going back through the set of enlarged figures, sequentially making the output of each problem be the input data for the next stage. EGN2 needs only to know the ratio of the scale factors and the offset of the origin to transform the output data from one stage to the input for the next.

Accordingly, fig. 6 shows the trajectories using the final conditions from fig. 5 as initial conditions. Figure 7 uses the output from the run in fig. 6 for initial conditions. Finally, fig. 8 uses the final conditions from fig. 7 to show the trajectories through the entire length of the original configuration.

2.1. Emission Models

It is beyond the scope of this paper to study the various emission models. However, it is interesting to consider that these high-resolution simulations may give some information as to which model is correct. Two very simple models are:

- (1) a whisker or bump, as was shown above, causes field enhancement sufficient to give the observed current; and
- (2) a surface contaminant such as an oxide layer causes a local reduction in the effective work function, as described by Latham [5].

It appears quite clear that the field enhancement due just to the shape of the sharp field emitters is not sufficient to cause significant emission, without one or both of the above conditions or some other mechanism to enhance the emission. In the following paragraphs we will consider the trajectory implications of the two options, and finally we will propose that the actual mechanism may require a combination of both models.

In a uniform field the field enhancement at the tip of a hemispherical bump is a factor of three. This enhancement is independent of the radius of the bump. In fig. 9 we show the surface field distribution both for the bump in fig. 5 and for a bump with double the radius. Although there is some lack of smoothness in the plots due to the mesh structure, the obvious regularity and the fact that both curves have the same maximum demonstrate the accuracy of the method.

The obvious characteristic of emission from a small bump or whisker is that the beam spreads quickly into a large angular cone. In our simulation we can best deal with

a bump on the axis, while in practice there would more likely be several bumps scattered over the surface of the point. There cannot be a large number of bumps, or the surface would again become smooth, but 10 to 100 bumps of various sizes seems possible. The emission pattern shown for one bump would then be repeated and overlaid a number of times. This would result in a large, fairly uniformly illuminated region of the anode with an intensity pattern that would generally resemble a Gaussian curve. The angular divergence of the spot at a distance from the tip is about ten degrees, as shown in fig. 8.

Since the bump is of atomic dimensions, it could be that electrons prefer to tunnel from the tip of the bump; in effect, the work function varies around the atom, being at its lowest at the tip. This is a quantum mechanical problem that needs to be addressed analytically [6].

Short whiskers with hemispherical ends, as shown in fig. 10, have slightly larger divergent angles, primarily because the emission is initiated at larger angles since the enhanced field continues around the point farther. Table 1 shows the peak field, emitted current, and divergence angle for various whisker lengths, where the work function is 4.5 eV in all cases. In practice, the observed angle of divergence is about two degrees, and is smaller for whiskers with adsorbed barium atoms than for uncontaminated whiskers [7].

If we consider that a small region with atomic dimensions of a few angstroms might emit with an anomalously low work function from a smooth microsurface, then emission from the tip would appear as modeled in fig. 11. A reasonable number of such sites could be emitting, causing an emission pattern with numerous hot spots. Using a spot about 6 Å in diameter, as shown in fig. 11, the emission was about 0.1 μA with a work function of only 2.0 eV. A statistically significant number of such sites—perhaps ten or more—would be required per tip in order to account for the observed emission, or indeed to assure that there would be any emission at all.

If as suggested above a few geometric enhancements also were to have an anomalously low work function segment, then it is not necessary that the work function be extremely low. These enhanced regions must in general be somewhat larger than the emitting spot, or again the emission pattern would be very spread out. There could not be very many such regions per tip, simply because of the lack of room, but each tip could have more than one site. The gain of three in field strength greatly augments the emission function so that, for example, in the case of the model shown in fig. 12 with a 1 nm radius bump and a work function of 3 eV, the emission is about 1 μ A. The beam from fig. 12 was carried through the intermediate stages, as demonstrated previously, and finally gave the result shown in fig. 13. The spread is still significant due to the small radius of the bump, but the extent of it is reduced to about five degrees. As the radius of the small bump is increased, the divergence approaches the small spread shown in fig. 11, which would also agree with the observation of small hot spots with two-degree divergence.

3. EGN2 Techniques

In this section we describe some of the special techniques that were used to make the high-resolution simulations with EGN2. The reader should refer to the Instructions for EGN2 and POLYGON for a more general application of the data described here.

For the output shown in fig. 2, EGN2 was asked for the equipotentials to be initiated in the uniform field region at $R=30$, by setting $EQUIPR=30$. EGN2 was also asked for a single field line, selected to start at a point along the cone such that the line would terminate near the end, to the gate electrode. Field lines in EGN2 are obtained by forcing the momentum of the trajectories to be reset to zero after each iterative step. This condition is signaled to EGN by setting the particle mass to a negative number; e.g., $MASS=-1$. Data for a trajectory is saved in the input format for POLYGON if

MASS=-1 and IPBP = 1, assuming only one trajectory. The IPBP signals EGN2 to record all the data for every step of up to six particles with ray numbers given in the format IPBP= n_1, n_2 , etc. Similarly, the coordinates for the equipotential line is saved if the line is called for by the parameter EQZLST, which is the Z-coordinate of a point at R=EQUIPR. Finally, all this data is saved in the output file, which can be printed or scanned on a monitor. An editor can be used to extract the necessary segments of the field line and the equipotential line to form the boundary input data for POLYGON. As an added convenience, the data for a field line and an equipotential line (if called as described above) are saved instead in a separate file if a file designation is placed in the sixth position of the command line calling EGN2. The command line has the following format: EGN2 inputfile outputfile plotfile cardfile binaryfile polyfile.

The choice of the starting points for the equipotential line and the field line determines the directions for these lines, and thus the sequence of points. They must be specified so that the lines go in the right direction (which is why EQUIPR=30 was used) to avoid a large editing job inverting the sequence of these points. Note that equipotential lines start both "up" and "down" when they are called. The editing task for preparing the new dataset for POLYGON consists of deleting the rest of the boundary from the initial input dataset for POLYGON, saving only the part needed (in this case only that part for the tip of the cone), and then adding in the desired segment of the field line and the equipotential, respectively. Some care is needed at the intersection of these two segments to avoid confusing POLYGON. The last line of POLYGON input consists of four numbers: RO, ZO, SFR, and SFZ where RO and ZO define a new origin and SFR and SFZ define the zoom scale factors. In this case we used SFR=SFZ=10 and RO=0. The number ZO was chosen so as not to waste too much space (equal to the Z-value of the starting point of the field line in this case) only because the plots get strange looking if the origin is far from the region of interest. The ZO value will be

needed again when the coordinates are shifted back, to permit continuations of the runs for ray tracing. Thus it is useful to record the ZO's and helpful to use simple numbers. Note that the transformation equations are of the form:

$$ZNEW = (ZOLD + ZO)*SFZ \quad .$$

In some cases there is not enough detail in the input boundary set to POLYGON to result in an adequate result. In these cases a simple stratagem is to use the file PANZOOM.IN, which POLYGON creates to run with the transformed input data. This file can be edited to be an ordinary POLYGON input file, with adequate detail but without the PANZOOM data line. This trick was used in the two enlargements of a factor of ten, as shown earlier.

4. Conclusions

Enhancements to the electron optics program EGN2 have enabled it to be used for high-resolution simulations of electron trajectories from field-emitting points with radii of a few hundred angstroms. It is anticipated that this method of simulation will prove useful for testing hypotheses for the origination of field emission from very sharp tips, which is important for vacuum microelectronic devices [8] (including tunneling microscopes) and for the design of electrostatic lenses used with such devices. An example for the use of such a lens with a field emitter is shown in fig. 14.

To simulate the observation that the emission from such tips actually comes from one or a few atomic sites [2,7], it was postulated that the localized emission was either due to field enhancement by a single protruding atom, or by the lowering of the work function at a given site due to a single nonprotruding impurity atom imbedded in the surface. Using the Fowler-Nordheim theory and assuming a uniform work function around an atomic bump, a divergence angle of ten degrees or more is predicted. For the imbedded

atom of low work function, an angular spread of about two degrees is predicted, in substantial agreement with observations where the divergence angle appears to vary with the type of atom from whence the electrons are streaming [7]. Combining the imbedded atom with a small bump gives enhanced emission with divergence angles that are between the two extremes described here. Clearly, it may be extending the Fowler–Nordheim theory beyond its scope to apply it directly to atomic sites [6], but it should be straightforward to apply any new developments in tunneling theory to this computer model.

References

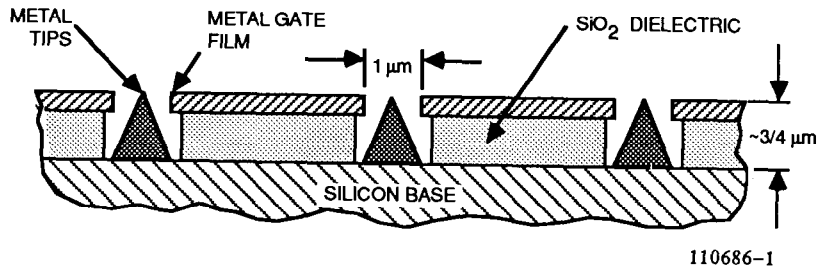
- [1] R. H. Fowler and L. W. Nordheim, *Proc. Roy. Soc.*, **A119** (1928) 173.
- [2] C. A. Spindt, I. Brodie, L. Humphrey, and E. R. Westerberg, *J. Appl. Phys.* **47** (1976) 5248.
- [3] W. B. Herrmannsfeldt, EGUN—An Electron Optics and Gun Design Program, SLAC Report-331 (1988).
- [4] R. Becker, *Nucl. Instrum. Methods* **B42** (1989) 162.
- [5] R. V. Latham, *High Voltage Vacuum Insulation: The Physical Basis* (Academic Press, 1981).
- [6] R. H. Cutler, T. E. Feuchtwang, Z. Huang, and T. Sullivan, *Tunneling Theory and Vacuum Microelectronics*, in American Institute of Physics Conference Series 99 (1989) 121–123.
- [7] I. Brodie, “The Visibility of Atomic Objects in the Field Electron Microscope,” in *Surface Science* **70** (1978) 186–196.
- [8] American Institute of Physics Conference Series 99 (1989).

Table 1. Emission from Whiskers.

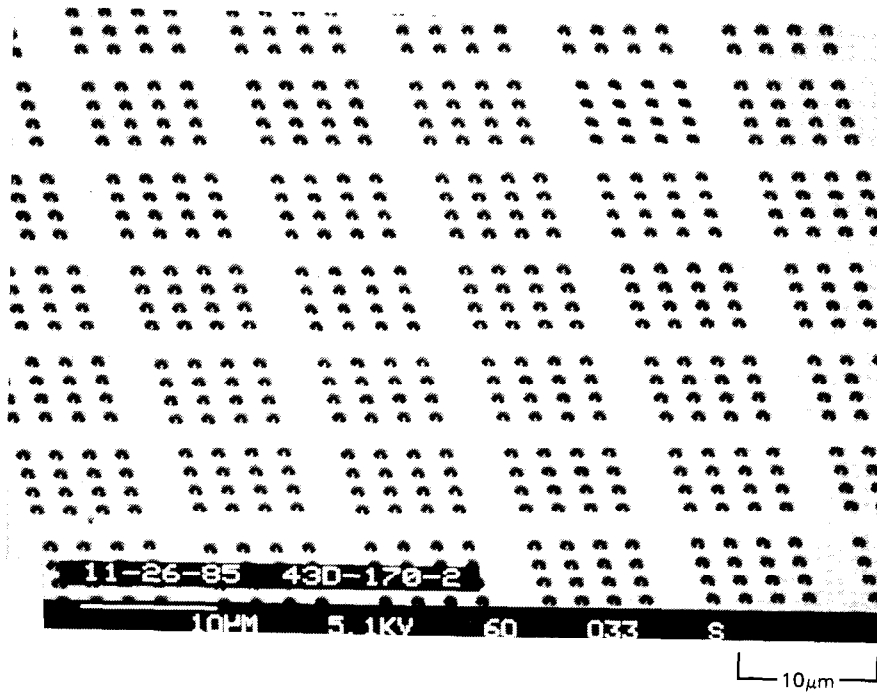
Length/radius	0	1	2	3	5
Peak field (10^8 V/cm)	0.5	0.68	0.84	1.02	1.3
Emission (μ A)	0.00056	0.054	0.53	2.6	18.3
Diversion (degrees)	9.7	16.5	18.2	20.1	23

Figure Captions

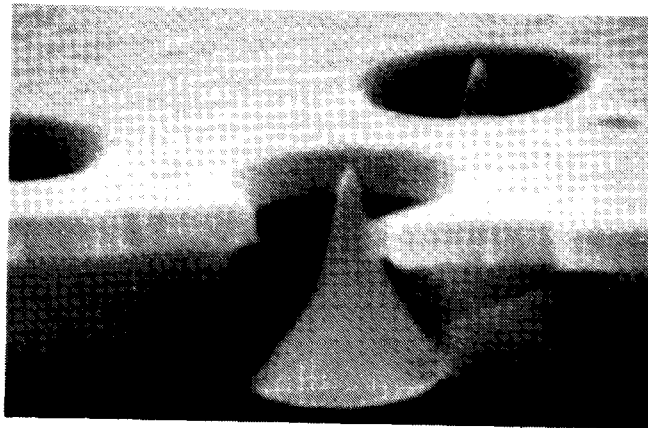
1. A microphotograph of a gated field emitter array.
2. The EGN2 model of a gated field emitter with a mesh unit of $0.05 \mu\text{m}$.
3. Enlarged segment from fig. 2 with a mesh unit of 5 nm .
4. Enlarged segment from fig. 3 with a mesh unit of 5 \AA .
5. Enlarged segment from fig. 4 with a mesh unit of 1 \AA . Emission calculations made using the Fowler–Nordheim Equation.
6. Particles from fig. 5 are reinjected into the next larger-scale segment.
7. Particles from fig. 6 are reinjected into the next larger-scale segment.
8. Particles from Fig. 7 continue through the original configuration.
9. Electric field around the 0.5 nm bump shown in fig. 5 and also for the 1.0 nm radius bump shown in fig. 12.
10. Emission pattern from a whisker with $\text{length}/\text{radius} = 3$.
11. Emission pattern from a small region of a smooth surface.
12. Emission from a small area on the tip of a 1 nm radius bump.
13. Beam from fig. 12 transported with a divergence angle of about five degrees.
14. Field emission tip with a focusing electrode to produce a parallel beam.



(a) SCHEMATIC OF A SPINDT CATHODE ARRAY

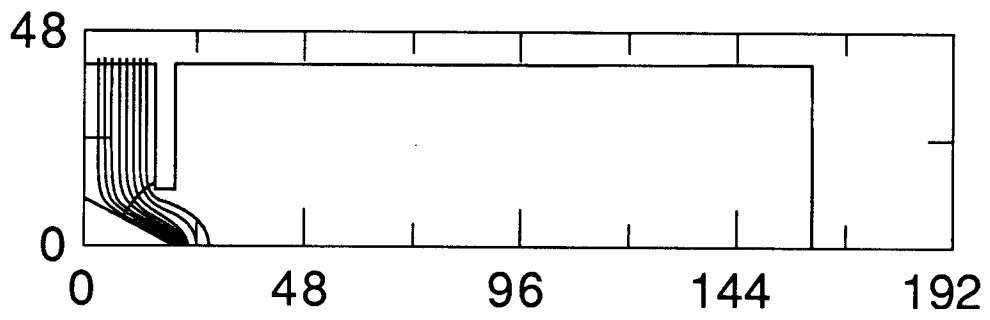


(b) SEM MICROGRAPH OF SPINDT CATHODE ARRAY



(c) SEM MICROGRAPH OF INDIVIDUAL SPINDT CATHODE

Fig. 1



3-90

6591A2

Fig. 2

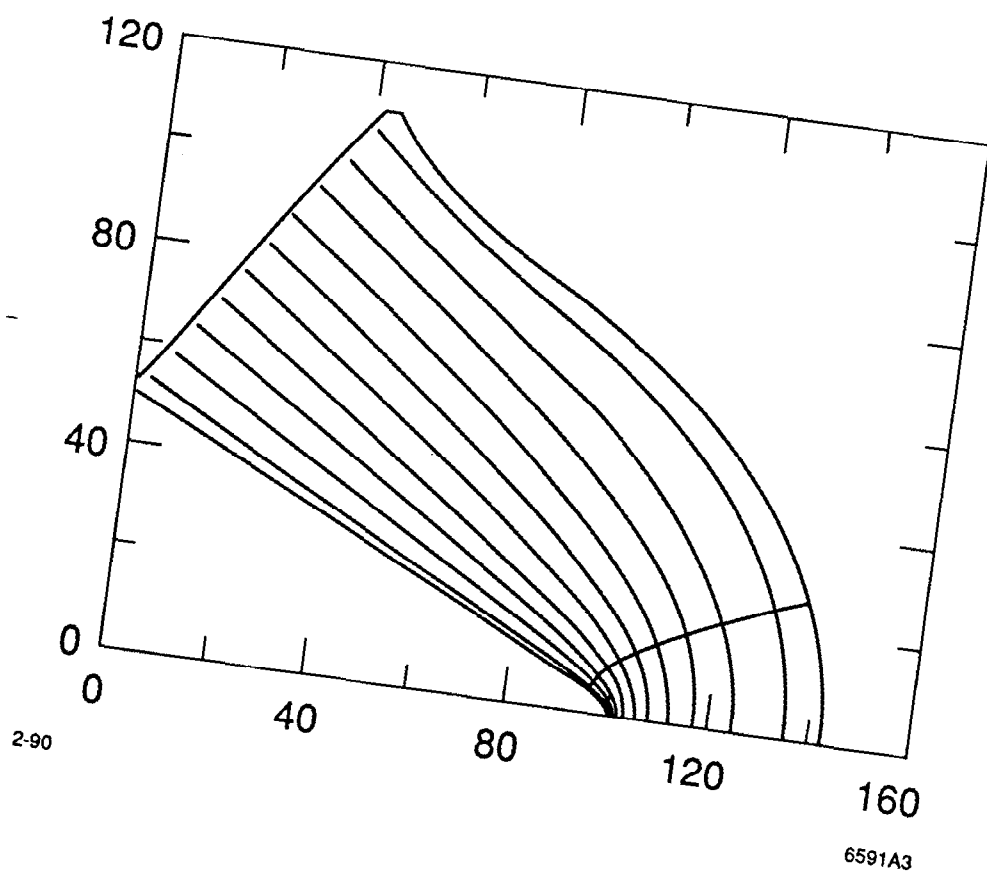
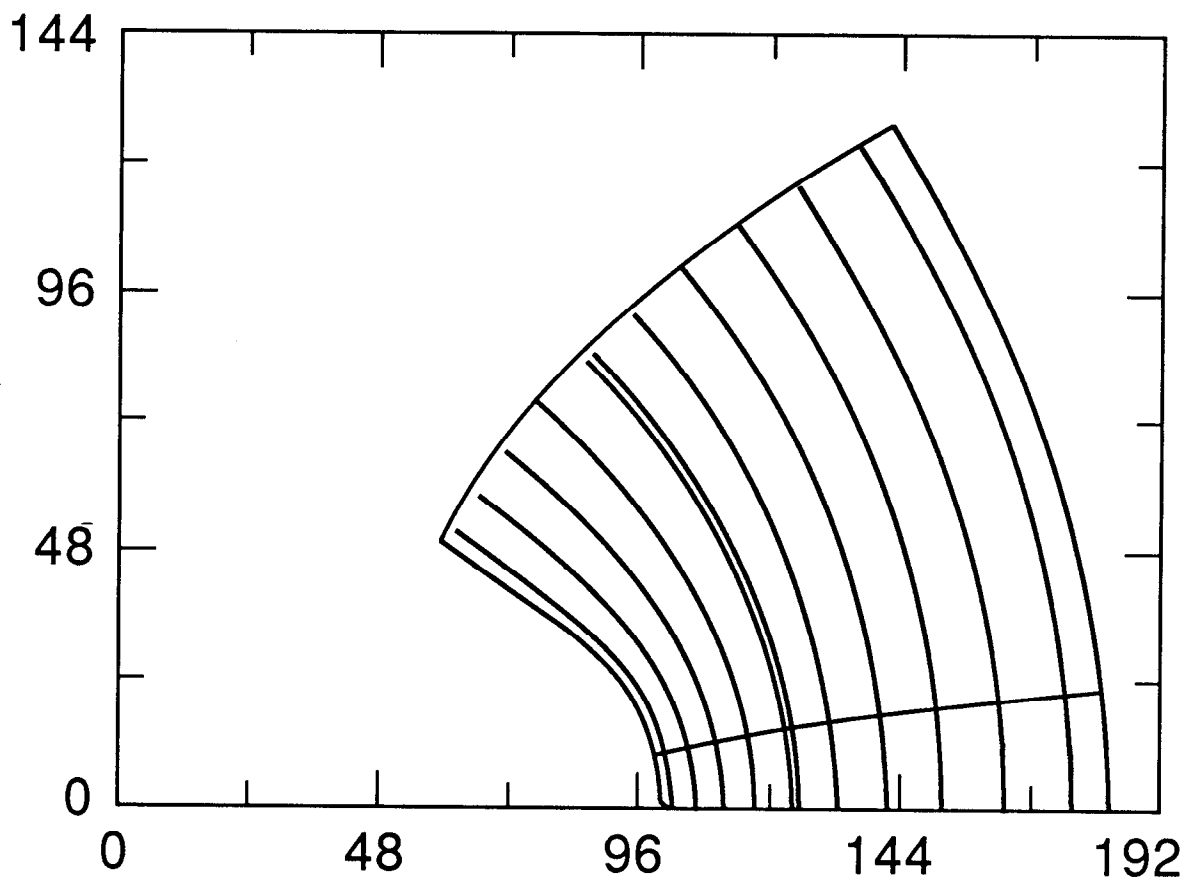


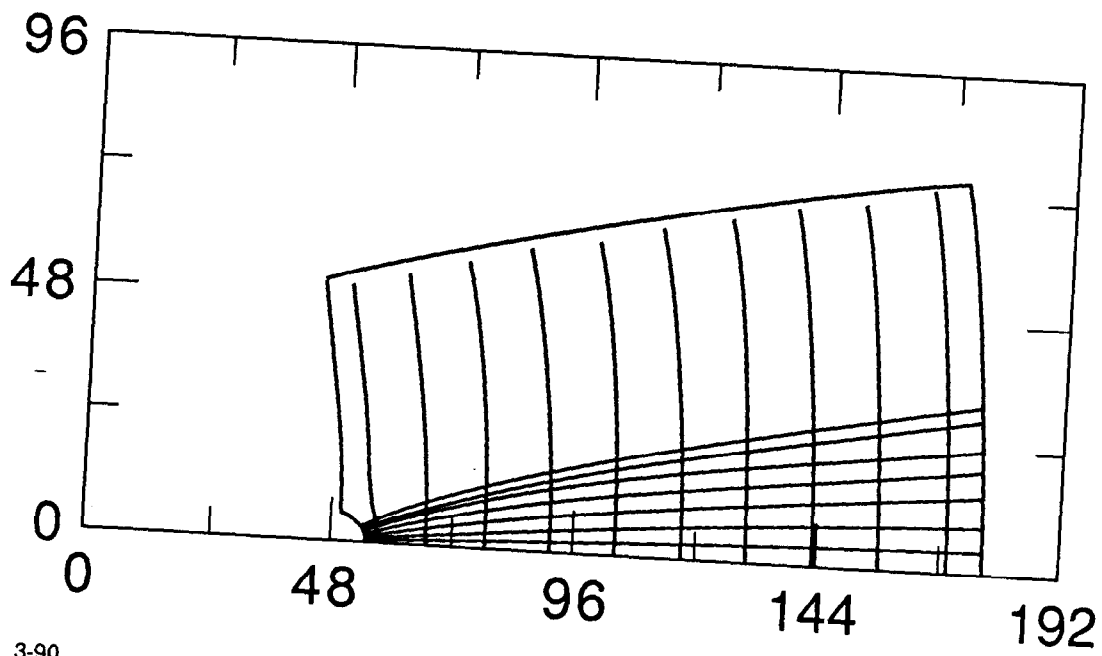
Fig. 3



2-90

6591A4

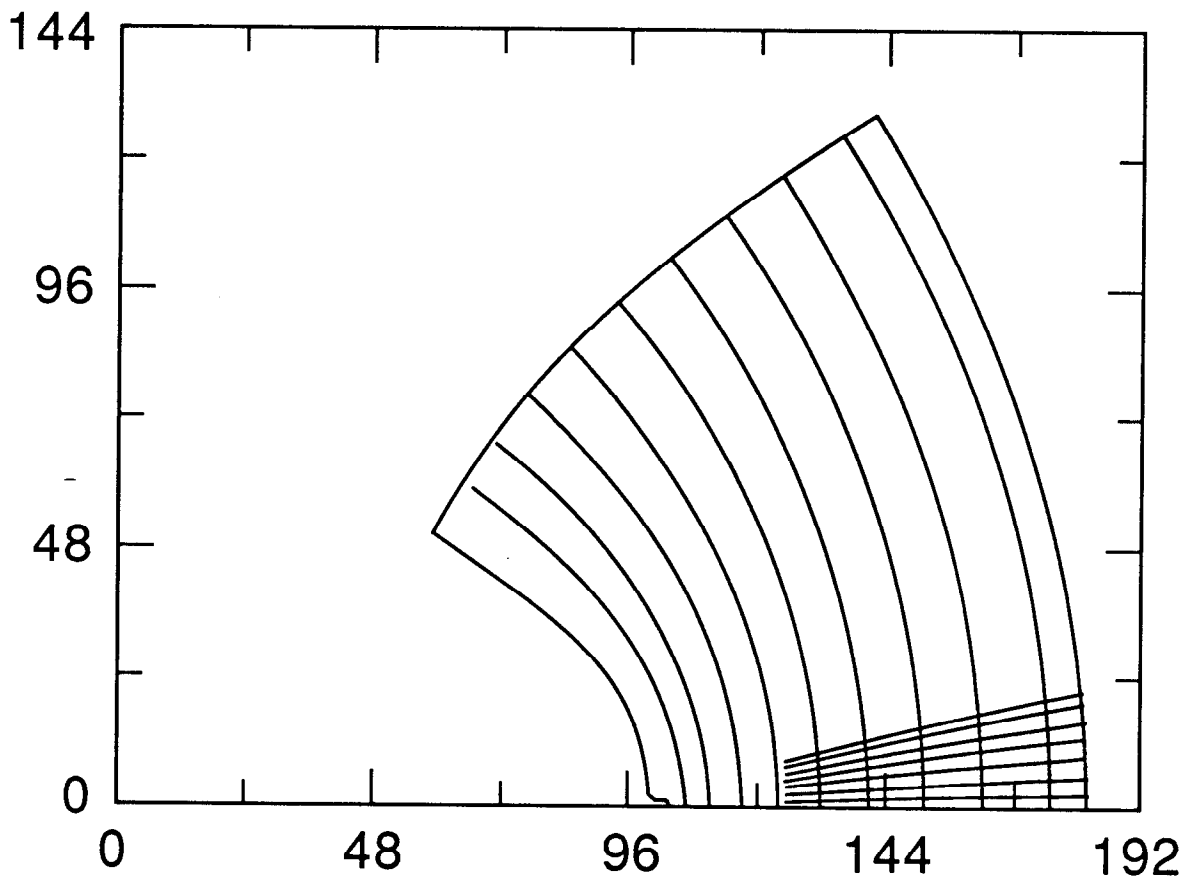
Fig. 4



3-90

6591A5

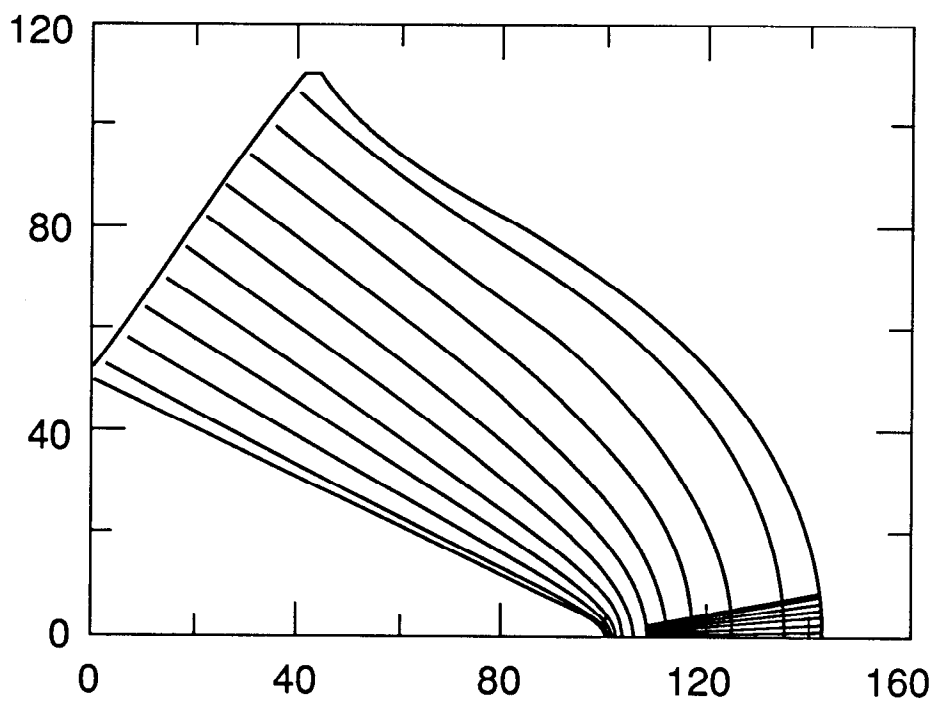
Fig. 5



2-90

6591A6

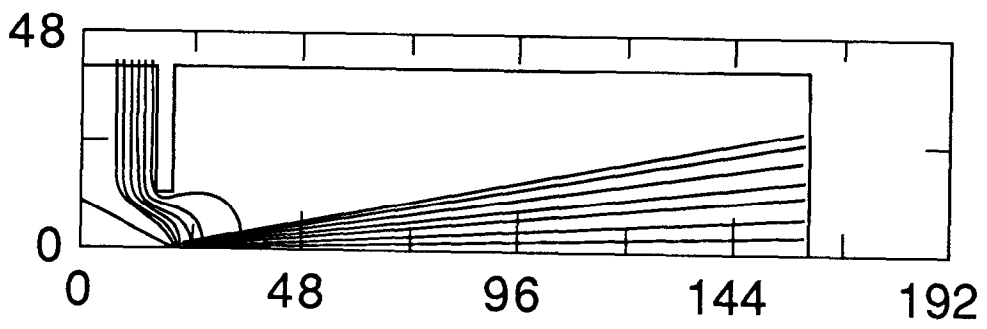
Fig. 6



2-90

6591A7

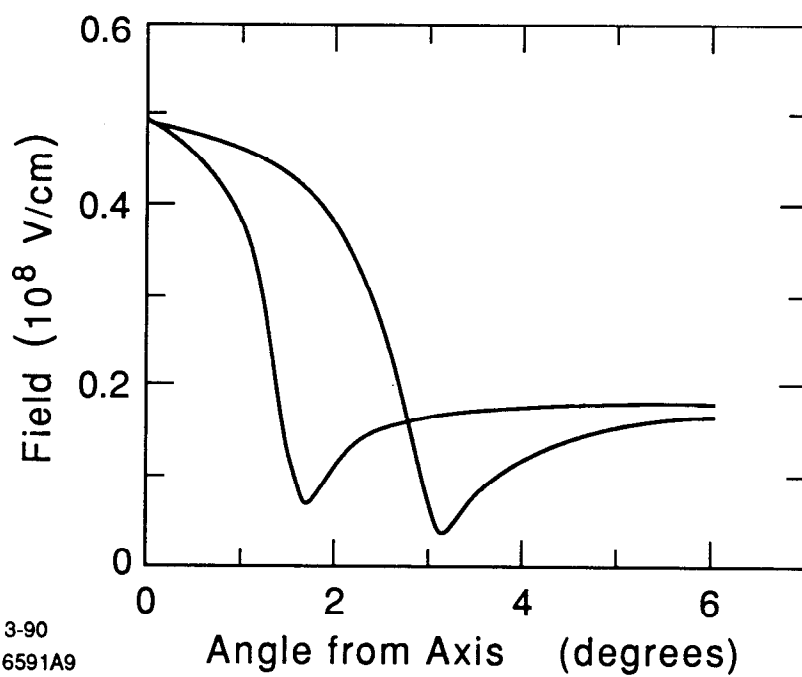
Fig. 7



3-90

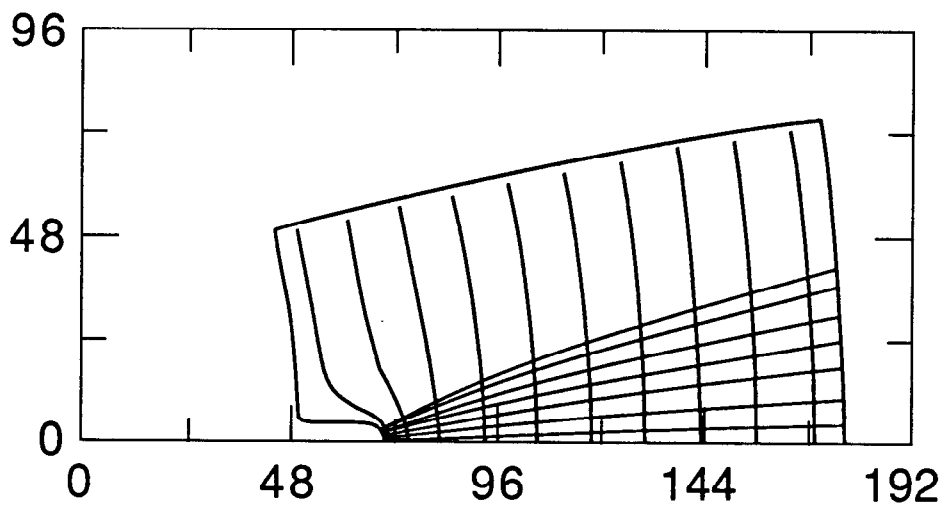
6591A8

Fig. 8



3-90
6591A9

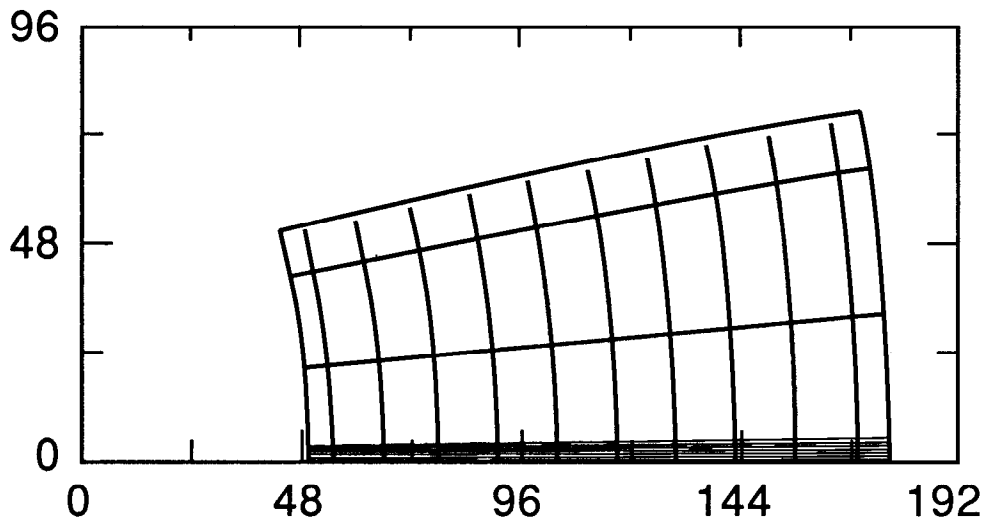
Fig. 9



3-90

6591A10

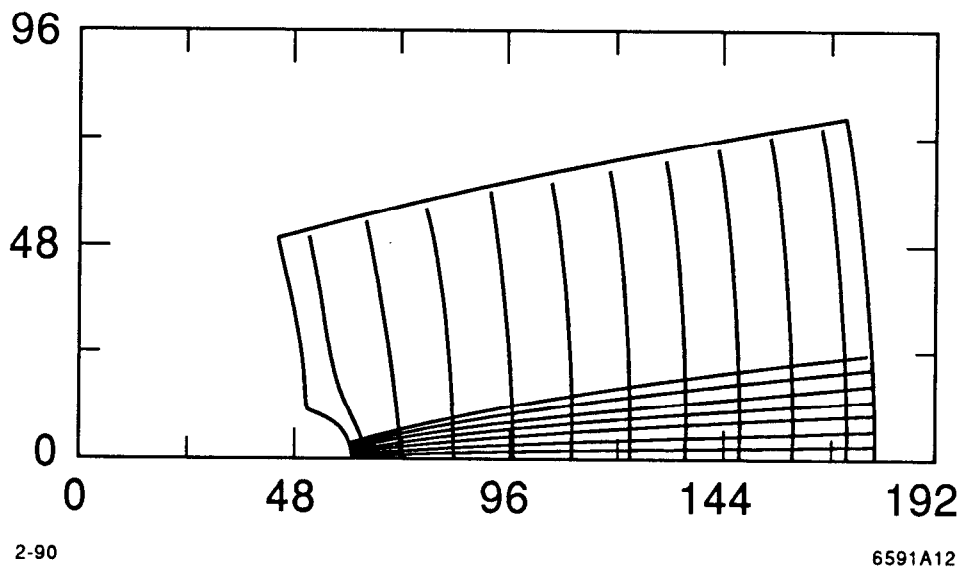
Fig. 10



4-90

6591A11

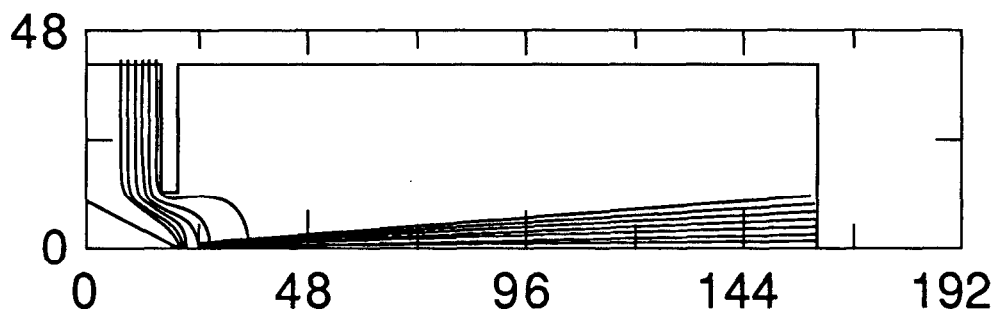
Fig. 11



2-90

6591A12

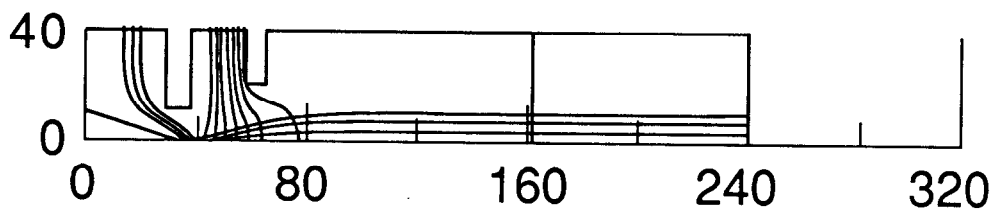
Fig. 12



3-90

6591A13

Fig. 13



3-90

6591A14

Fig. 14